A Chromosome-level Sequence Assembly Reveals the Structure of the *Arabidopsis thaliana* Nd-1 Genome and its Gene Set

Boas Pucker[1], Daniela Holtgräwe[1], Kai Bernd Stadermann[1], Katharina Frey[1], Bruno Huettel[2], Richard Reinhardt[2] and Bernd Weisshaar[1*]

[1] Bielefeld University, Faculty of Biology & Center for Biotechnology, Bielefeld, Germany

[2] Max Planck Genome Centre Cologne, Max Planck Institute for Plant Breeding Research, Cologne, Germany

[*] Corresponding author (BW)

Email addresses:
BP: bpucker@cebitec.uni-bielefeld.de
DH: dholtgra@cebitec.uni-bielefeld.de
KS: kstaderm@cebitec.uni-bielefeld.de
KF: katharina.frey@uni-bielefeld.de.
BH: huettel@mpipz.mpg.de
RR: reinhardt@mpipz.mpg.de
BW: bernd.weisshaar@uni-bielefeld.de

ORCIDs
BP: https://orcid.org/0000-0002-3321-7471
DH: https://orcid.org/0000-0002-1062-4576
KS: https://orcid.org/0000-0002-8036-1492
BW: https://orcid.org/0000-0002-7635-3473

Abstract

Background

In addition to the BAC-based reference sequence of the accession Columbia-0 from the year 2000, several short read assemblies of THE plant model organism *Arabidopsis thaliana* were published during the last years. Also, a SMRT-based assembly of Landsberg *erecta* has been generated that identified translocation and inversion polymorphisms between two genotypes of the species.

Results

Here we provide a chromosome-arm level assembly of the *A. thaliana* accession Niederzenz-1 (AthNd-1_v2c) based on SMRT sequencing data. The best assembly comprises 69 nucleome sequences and displays a contig length of up to 16 Mbp. Compared to an earlier Illumina short read-based NGS assembly (AthNd-1_v1), a 75 fold increase in contiguity was observed for AthNd-1_v2c. To assign contig locations independent from the Col-0 gold standard reference sequence, we used genetic anchoring to generate a *de novo* assembly. In addition, we assembled the chondrome and plastome sequences.

Conclusions

Detailed analyses of AthNd-1_v2c allowed reliable identification of large genomic rearrangements between *A. thaliana* accessions contributing to differences in the gene sets that distinguish the genotypes. One of the differences detected identified a gene that is lacking from the Col-0 gold standard sequence. This *de novo* assembly extends the known proportion of the *A. thaliana* pan-genome.

Background

Introduction

Arabidopsis thaliana became the most important model for plant biology within decades due to properties valuable for basic research like short generation time, small footprint, and a small genome [1]. Shortcomings of the BAC-by-BAC assembled 120 Mbp long Col-0 gold standard sequence [2] are some missing sequences and gaps in almost inaccessible regions like repeats in the centromeres [3, 4], at the telomeres and throughout NORs as well as few mis-assemblies [5, 6]. Information about genomic differences between *A. thaliana* accessions were mostly derived from short read data [7-9]. Only selected accessions were sequenced deep enough and with sufficient read length to reach almost reference-size assemblies [7, 10-15]. While the identification of SNPs can be based on short read mappings, the identification of structural variants had an upper limit of 40 bp for most of the investigated accessions [9]. Larger insertions and deletions, which will often result in presence/absence variations of entire genes, are often missed in short read data sets but are easily recovered by long read sequencing [14-16]. *De novo* assemblies based on long sequencing reads are currently emphasized to resolve structural variants without an upper limit and to facilitate *A. thaliana* pan-genomics. Even a fully complete Col-0 genome sequence would not reveal the entire diversity of this species, as this accession is assumed to have a relatively small genome compared to other *A. thaliana* accessions.

The strong increase in the length of sequencing reads that was technically realized during the last years is enabling new assembly approaches [17, 18]. Despite the high error rate of 'Single Molecule, Real Time' (SMRT) sequencing, the long reads significantly improve contiguity of *de novo* assemblies due to an efficient correction of the almost unbiased errors [19-21], provided that sufficient read coverage is available. SMRT sequencing offered by PacBio results routinely in average read lengths above 10 kbp [10, 22, 23]. These long reads were incorporated into high quality hybrid assemblies involving Illumina short read data [14, 23], but increasing sequencing output supports the potential for so called 'PacBio only assemblies' [10-12, 15, 20]. Oxford Nanopore Technology's (ONT) sequencing provides

even longer reads with recent reports of longest reads over 2 Mbp [24]. However, the error rate of 5-15% [25] is still an issue in plant genome assembly although it has been shown that a high contiguity assembly is possible for *A. thaliana* [15].

Here we provide a SMRT sequencing-based *de novo* genome assembly of Nd-1 comprising contigs of chromosome-arm size anchored to chromosomes and oriented within pseudochromosome sequences based on genetic linkage information. The application of long sequencing reads abolished limitations of short read mapping and short read assemblies for genome sequence comparison. Based on this genome sequence assembly, we identified genomic rearrangements between Col-0 and Nd-1 ranging from a few kbp up to one Mbp. Gene duplications between both accessions as well as lineage specific genes in Nd-1 and Col-0 were revealed by this high quality sequence. The current assembly version outperforms the Illumina-based version (AthNd-1_v1) about 75 fold with respect to assembly contiguity calculated with respect to number of contigs [13] and is in the same quality range as the recently released L*er* and KBS-Mac-74 genome sequence assembly [14, 15].

Methods

Plant material

Niederzenz-1 (Nd-1) seeds were obtained from the European Arabidopsis Stock Centre (NASC; stock number N22619). The DNA source was the same as described earlier [13].

DNA extraction

The DNA isolation procedure was based on previously published protocols [12, 26] and started with 5 g of frozen leaves which were homogenized by grinding. Samples were mixed in a 1:10 ratio with extraction buffer (300mM Tris pH8.0, 25mM EDTA, 2M NaCl, 2% polyvinylpyrrolidone (PVP), 2% hexadecyltrimethylammonium bromide (CTAB)) and incubated at 65°C for 30 minutes with six inversions to mix the samples again. After five minute spinning at 5,000xg, the supernatant was transferred and mixed with one volume of

chlorophorm/isoamylalcohol (24:1). Again, the upper phase was transferred after repetition of the centrifugation step for ten minutes. RNA was removed by adding 30µL RNase A (10mg/ml) and incubation for 30 minutes at 37°C. Addition of chlorophorm/isoamylalcohol, centrifugation and transfer of supernatant were repeated. One volume of isopropanol and 0.1 volumes of 3M NaOAc (pH 5.2) were added and mixed. DNA was precipitated by incubating at -80°C for 30 minutes and spinning for 45 minutes at 5,000g and a final ethanol wash step was performed. Finally, 500µl of 10mM Tris/HCl (pH 8.0) were added and samples were incubated over night at 4°C for resuspension.

Library preparation and sequencing

Sequencing was performed using PacBio RS II (Menlo Park, CA, USA). Five microgram high molecular weight DNA without further fragmentation was used to prepare a SMRTbell library with PacBio SMRTbell Template Prep Kit 1 (Pacific Biosciences, Menlo Park, CA, USA) according to the manufacturer's recommendations. The resulting library was size-selected using a BluePippin system (Sage Science, Inc. Beverly, MA, USA) to enrich for molecules larger than 11 kbp. The recovered library was again damage repaired and then sequenced on a total of 25 SMRT cells with P6-C4v2 chemistry and by MagBead loading on the PacBio RSII system (Pacific Biosciences, Menlo Park, CA, USA) with 360 min movie length.

Assembly parameters

A total of 1,972,766 subreads with an N50 read length of 15,244 bp and containing information about 16,798,450,532 bases were generated. Assuming a genome size of 150 Mbp, the data cover the genome at 112 fold.

Read sequences derived from the plastome [GenBank: AP000423.1] or chondrome [GenBank: Y08501.2] were extracted from the raw data set by mapping to the respective sequence of Col-0 as previously described [27]. Canu v1.4 [28] was used for the assembly of the organell genome sequences. Beside default parameters, a genome size of 0.37 Mbp for the chondrome and 0.167 Mbp for the plastome were assumed in the assembly process.

Scaffolding of initial contigs was performed with SSPACE-LongRead v1.1 [29] (parameters: -a 0 -i 70 -k 3 -r 0.3 -o 10). The quality of both assemblies was checked by mapping of NGS reads from Nd-1 [13] and Col-0 [30]. Manual inspection and polishing with Quiver v.2.3.0 (parameters: minSubReadLength=500, readScore>80, minLength=500, maxHits=10, maxDivergence=30, minAnchorSize=12, --maxHits=1, --minAccuracy=0.75, --minLength=50, --algorithmOptions="-useQuality", --seed=1, --minAccuracy=0.75, --minLength=50, --concordant --algorithmOptions="-useQuality", minConfidence=40, minCoverage=5, diploidMode=False) [12] let to the final sequences. The start of the Nd-1 plastome and chondrome sequences was set according to the corresponding Col-0 sequences to ease comparisons. Finally, small assembly errors were corrected via CLC basic variant detection (ploidy=2; coverage<100,000; minimalCoverage=5; minimalCount=5; minimalFrequency=0.2) based on mapped Illumina paired-end reads (SRX1683594, [13]) and PacBio reads. Sequence properties like GC content and GC skew were determined and visualized by CGView [31].

A total of 166,600 seed reads spanning 4,500,092,354 nt (N50 = 26,295 nt) and covering the expected 150 Mbp genome sequence were used for the assembly thus leading to a coverage of 30 fold (see AdditionalFile1 for details). Assemblies were performed with Canu [28], FALCON [12], Flye [32] and miniasm [33]. These assemblies are named Ath-Nd1_v2 with an assembler specific suffix (c=Canu, f=FALCON, y=Flye, m=miniasm).

All available SMRT sequencing reads were subjected to Canu v.1.7.1 [28] for read correction, trimming, overlap detection, and *de novo* assembly (see AdditionalFile2 for parameters). Contigs with a length below 50 kb were discarded to avoid artifacts. The remaining contigs were checked for contaminations with bacterial sequences and organell genome sequences as previously described [13]. BWA-MEM v0.7.13 [34] was used with default parameters and -m to map Nd-1 Illumina reads [13] to this assembly. The coverage depth was extracted from the resulting BAM file as previously described [35] and used to

support the identification of plastome and chondrome contigs. Pilon v.1.22 [36] was applied twice with default parameters for polishing of the assembly.

Release version 1.7.5 of the FALCON assembler https://github.com/PacificBiosciences/FALCON/ [12] was used for a *de novo* assembly (see AdditionalFile3 for parameters) of the nuclear genome sequence. Resulting contigs were checked for contaminations with bacterial sequences and organell genome sequences as previously described [13]. Small fragments with low coverage were removed prior to polishing and error correction with Quiver [12].

SMRT sequencing reads were corrected via Canu and subjected to miniasm v0.3-r179 [33] for *de novo* assembly. Illumina reads were mapped with BWA-MEM for two rounds of polishing via Pilon as described above. The assembly was reduced to nucleome contigs as described above for the Canu assembly.

Flye v2.3.1 [32] was deployed on the subreads with an estimated genome size of 150 Mbp. The resulting assembly was polished twice via Pilon and reduced to nucleome contigs as described above for the Canu assembly.

Construction of pseudochromosomes based on genetic information

All 26 contigs of Ath-Nd1_v2f were sorted and orientated based on genetic linkage information derived from 63 genetic markers (AdditionalFile4, AdditionalFile5, AdditionalFile6), which were analyzed in about 1,000 F2 plants, progeny of a reciprocal cross of Nd-1xCol-0 and Col-0xNd-1. Genetic markers belong to three different types: (1) fragment length polymorphisms, which can be distinguished by agarose gel electrophoresis, (2) small nucleotide polymorphisms which can be distinguished by Sanger sequencing and (3) small nucleotide polymorphisms, which were identified by high resolution melt analysis. Design of oligonucleotides was performed manually and using Primer3Plus [37]. DNA for

192 genotyping experiments was extracted from *A. thaliana* leaf tissue using a
193 cetyltrimethylammonium bromide (CTAB) based method [38]. PCRs were carried out using
194 GoTaq® G2 DNA Polymerase (Promega) generally based on the suppliers' protocol. The
195 total reaction volume was reduced to 15 µl and only 0.2u of the polymerase were used per
196 reaction. Sizes of amplicons generated were checked on agarose gels. If required, samples
197 were purified for sequencing by ExoSAP-IT (78201.1.ML ThermoFisher Scientific) treatment
198 as previously described [39]. Sanger sequencing on ABI3730XL was applied to identify
199 allele-specific SNPs for the genotyping. Manual inspection of gel pictures and
200 electropherograms lead to genotype calling. High resolution melt analysis was performed on
201 a CFX96 Touch Real-Time PCR Detection System (BioRad) using the Precision Melt
202 Supermix according to suppliers instructions (BioRad). All data were combined, processed
203 by customized Python scripts to calculate recombination frequencies between genetic
204 markers. Linkage of genetic markers provided information about relationships of assembled
205 sequences. The north-south orientation of the chromosomes was transferred from the
206 reference sequence based on RBH support. Contigs were joined to pseudochromosome
207 sequences for Ath-Nd1_v2f. Subsequently, positioning was transferred to the 69 contigs of
208 the Canu assembly to create pseudochromosome sequences for AthNd-1_v2c
209 (AdditionalFile7).
210 Since the assemblies except Ath-Nd1_v2f contain smaller contigs in the range of 50-100 kb,
211 anchoring via genetic linkage information was not feasible. Therefore, these short contigs
212 were placed based on best BLASTn matches to the TAIR9 sequence (i.e. the Col-0 gold
213 standard reference) and integrated into pseudochromosomes as previously described [13].
214 We used the TAIR9 sequence, because this is the sequence basis of the structural and
215 functional annotation provided in TAIR9, TAIR10 and Araport11 [40]. Since the total length of
216 the TAIR9 sequence exceeds that of the Ath-Nd1_v2f assembly, TAIR9 was selected for
217 anchoring of small contigs.
218 All data generated is stored in the PGP Repository [41] and is accessible via DOI
219 (https://doi.org/10.5447/IPK/2019/4).

220

221 **Genome structure investigation**

222 Characteristic elements of the Nd-1 genome sequence were annotated by mapping of known
223 sequences as previously described [13]. Fragments and one complete 45S rDNA unit were
224 discovered based on gi|16131:848-4222 and gi|16506:88-1891. AF198222.1 was subjected
225 to a BLASTn search for the identification of 5S rDNA sequences. Telomeric repeats were
226 used to validate the assembly completeness at the pseudochromosome end as well as
227 centromere positions as previously described [13].

228

229 **BUSCO analysis**

230 BUSCO v3 [42] was run with default parameters on the Nd-1 pseudochromosomes and on
231 the TAIR9 reference sequence to produce a gold standard for Arabidopsis. The
232 'embryophyta_odb9' was used as reference gene set.

233

234 **Genome sequence alignment**

235 Nd-1 pseudochromosome sequences were aligned to the Col-0 gold standard sequence [2]
236 via nucmer [43] and NucDiff [44] based on default parameters of NucDiff. Customized Python
237 scripts were deployed to process the results and to assess the genome-wide distribution of
238 differences. Spearman correlation coefficient was calculated using the implementation in the
239 Python module scipy to validate the indication of increased numbers of SV around the
240 centromeres.

241

242 **Gene prediction and RBH analysis**

243 AUGUSTUS v.3.3 [45] was applied to all four Nd-1 assemblies with previously optimized
244 parameters [39]. Afterwards, the identification of RBHs at the protein sequence level
245 between Nd-1 and Col-0 (Araport11, representative peptide sequences) was carried out with
246 a custom Python script as previously described [13]. Additionally, gene prediction was run on
247 the Col-0 gold standard sequence [2] as well as on the L*er* chromosome sequences [14].

Parameters were set as described before to generate two control data sets. Previously trimmed and filtered ESTs [13, 46] were matched via BLASTn [47] to the predicted mRNAs. Pairwise global alignments were constructed via MAFFT v.7.299b [48] to validate the annotation quality. After processing GCA_000001735.1 (Col-0), Ath-Nd-1_v2c, and the most recent L*er* assembly [14] with RepeatMasker v4 [49] all three were subjected to cactus [50] for alignment. CAT [51] was run on this alignment with the ENSEMBL v42 annotation of Col-0.

INFERNAL [52] with default parameters and based on Rfam13 [53] was applied to detect various non-coding RNA genes. In addition, tRNAscan-SE [54] with –G option was deployed to identify tRNA and rRNA genes. Overlaps between both methods were analysed.

Transposable element annotation

All annotated transposable element (TE) sequences of Araport11 (derived from TAIR) [40] were mapped via BLASTn to the Nd-1 assembly AthNd-1_v2c and against the Col-0 gold standard sequence. The top BLAST score for each element in the mapping against the TAIR9 reference sequence was identified. All hits against Nd-1 with at least 90% of this top score were considered for further analysis. Overlapping hits were removed to annotate a final TE set. All predicted Nd-1 genes which overlapped TEs with more than 80% of their gene space were flagged as putative protein encoding TE genes. In addition, RepeatModeler v.1.0.11 [49] was deployed to identify novel TE sequences in the Ath-Nd-1_v2c assembly.

Identification of gene space differences

Genes in insertions in Ath-Nd1_v2c were searched in the Col-0 gold standard sequence and vice versa. The BLAST results on DNA and peptide level indicated the absence of any truly novel genes thus indicating that presence/absence variants are the results of gene duplications. Apparent gene space differences could be caused by regions missing in the assembly. Therefore, Nd-1 (SRR2919279, SRR3340908, SRR3340909) [13] and Col-0 (SRR1810832, SRR1945757)[9, 30] Illumina sequencing reads were mapped to Ath-

Nd1_v2c via BWA MEM [34] using the -m flag to discard spurious hits. The sequencing read coverage depth was calculated via bedtools by a customized Python script [35]. Average coverage per accession was calculated as the median of all coverage values. Per gene coverage was calculated as the median of all coverage values at positions in the respective gene and normalized to the average coverage of the respective accession. To correct for accession specific mapability differences caused e.g. by sequence divergence from Nd-1, the resulting values were additionally normalized to the median of all per gene ratios. Genes were considered as duplicated in Col-0 if their relative coverage in Nd-1 was below 50 % of the Col-0 value. Genes with Nd-1 values above 150 % of the Col-0 value were considered duplicated in Nd-1. These cutoff values were validated based on experimentally validated gene differences. Corresponding AGIs were identified via BLASTp to transfer the functional annotation of Araport11 if possible. Following this initial identification, putative TE genes were removed based on the annotation or the overlap with annotated TE sequences (AdditionalFile8), respectively.

Sequencing data of 1,135 *A. thaliana* accessions [9] were retrieved from the Sequence Read Archive, mapped to Ath-Nd1_v2c, and processed as described above. Accessions displaying an average coverage below 10x were excluded from the following identification of presence/absence variations. GeneSet_Nd-1_v2.0 genes were classified as dispensable if their relative coverage was below 0.1 in more than 100 accessions. Remaining genes were classified as core or TE genes depending on their overlap with TE features (see TE annotation).

Validation of rearrangements and duplications

LongAmpTaq (NEB) was used for the generation of large genomic amplicons up to 18 kbp based on the suppliers' protocol. Sanger sequencing was applied for additional confirmation of generated amplicons. The amplification of small fragments and the following procedures were carried out with standard polymerases as previously described [13].

Investigation of collapsed region

The region around At4g22214 was amplified in five overlapping parts using the Q5 High Fidelity polymerase (NEB) with genomic DNA from Col-0. Amplicons were checked on agarose gels and finally cloned into pCR2.1 (Invitrogen) or pMiniT 2.0 (NEB), respectively, based on the suppliers' recommendations. Cloned amplicons were sequenced on an ABI3730XL by primer walking. Sequencing reads were assembled using CLC GenomicsWorkbench (v. 9.5 CLC bio). In addition, 2x250 nt paired-end Illumina reads of Col-0 [30] were mapped to correct small variants in the assembled contigs and to close a small gap between cloned amplicons.

Analysis of gaps in the Col-0 reference sequence

Flanking sequences of gaps in the Col-0 gold standard sequence were submitted to a BLASTn against the Ath-Nd-1_v2c genome sequence. Nd-1 sequences enclosed by hits of pairs of 30 kbp long flanking sequences from Col-0 were extracted. Homotetramer frequencies were calculated for all sequences and compared against the frequencies in randomly picked sequences. A Mann-Whitney U test was applied to analyze the difference between both groups.

Results

Nd-1 genome

Assemblies generated via Canu (Ath-Nd-1_v2c), FALCON (Ath-Nd-1_v2f), Flye (Ath-Nd-1_v2y) and miniasm (Ath-Nd-1_v2m) were compared based on numerous assembly statistics (Table 1). AthNd-1_v2f exceeds the previously reported assembly version AthNd-1_v1 by 2.5 Mbp, while reducing the number of contigs by a factor of about 200 to 26. AthNd-1_v2c is adding 6.9 Mbp to the previous assembly version (AthNd-1_v1), but at the expense of a higher number of contigs than AthNd-1_v2f. We selected AthNd-1_v2c that contains 69 contigs as the representative assembly which should be used for further comparison.

Pseudochromosomes of AthNd-1_v2f were constructed truly *de novo* from 3-7 contigs based on genetic linkage information. All 26 contigs were anchored based on 63 genetic markers, but precise positioning around the centromeres of chromosome 4 and 5 was ambigious. Pseudochromosomes reach similar lengths as the corresponding chromosome sequences in the Col-0 gold standard sequence. Pseudochromosomes for AthNd-1_v2c were generated by transferring orientation and position of large contigs from AthNd-1_v2f. The Nd-1 genome sequence AthNd-1_v2c contains complete 45S rDNA units on pseudochromosome 3 as well as several fragments of additional 45S rDNA units on all other pseudochromosomes (Fig. 1). Centromeric and telomeric repeat sequences as well as 5S rDNA sequences were detected at centromere positions. Completeness of most assembled sequences was confirmed by the occurrence of telomeric repeat sequences (Fig. 1). The high assembly quality and completeness of AthNd-1_v2c is supported by the detection of 98.2% of all embryophyta BUSCO genes – even one more than detected in the Col-0 gold standard sequence (AdditionalFile9).

The plastome and chondrome sequences comprise 154,443 bp and 368,216 bp, respectively (https://doi.org/10.5447/IPK/2019/4). A total of 148 small variants were identified from a global alignment between the Nd-1 and Col-0 plastome sequences. General sequence properties like GC content and GC skew (AdditionalFile10, AdditionalFile11) are almost identical to the plastome and chondrome of Col-0. Nevertheless, there are some rearrangements between the chondrome sequences of Nd-1 and Col-0.

Genome structure differences

Sequence comparison between AthNd-1_v2c and the Col-0 gold standard sequence revealed a large inversion on chromosome 4 involving about 1 Mbp (Fig. 2). The left break point is at 1,637,889 bp and the right break point at 2,708,850 bp on chromosome 4 (NdChr4). The inverted sequence is 120 kbp shorter than the corresponding Col-0 sequence. PCR amplification of both inversion borders (AdditionalFile12) and Sanger sequencing of the generated amplicons was used to validate this rearrangement.

The recombination frequency in this region was analyzed using the marker pair M84/M74. Only a single recombination was observed between these markers while investigating 60 plants. Moreover, only 8 recombination events in 108 plants were observed between another pair of markers, spanning a larger region across the inversion (AdditonalFile5). In contrast, the average recombination frequency per Mbp at the corresponding position on other chromosomes was between 12%, observed for M31/M32, and 18%, observed for M13/M14. Statistical analysis revealed a significant difference in the recombination frequencies between the corresponding positions on different chromosomes ($p<0.001$, prop.test() in R) supporting a reduced recombination rate across the inversion on chromosome 4.

Comparison of a region on Chr2, which is probably of mitochondrial origin (mtDNA), in the Col-0 gold standard sequence with the Nd-1 genome sequence revealed a 300 kbp highly divergent region (Fig. 3). Sequences between position 3.20 Mbp and 3.29 Mbp on NdChr2 of AthNd-1_v2c display low similarity to the Col-0 gold standard sequence, while there is almost no similarity between 3.29 Mbp and 3.48 Mbp. However, the length of both regions is roughly the same. Comparison against the L*er* genome sequence assembly revealed the absence of the entire region between 3.29 Mbp and 3.48 Mbp on chromosome 2. The Nd-1 sequence from this region lacks continuous similarity to any other region in the Col-0 or Nd-1 genome sequence. However, the 28 genes encoded in this region in Nd-1 show weak similarity to other Arabidopsis genes. Comparison of gene space sequences from this region against the entire Nd-1 assembly revealed some similarity on chromosome 3, 4, and 5 (AdditionalFile13).

An inversion on chromosome 3 of 170 kbp which was described between Col-0 and L*er* [14] is not present in Nd-1. The sequence similarity between Col-0 and Nd-1 is high in this region. In total, 2206 structural variants larger than 1 kbp were identified between Col-0 and Nd-1. The genome-wide distribution of these variants indicated a clustering around the centromeres (AdditionalFile14). A Spearman correlation coefficient of -0.79 ($p=1.1*10^{-27}$) was calculated for the correlation of the number of SVs in a given interval and the distance of this interval to the centromere (AdditionalFile15). Therefore, these large structural variants are

387 significantly more frequent in the centromeric and pericentromic regions. A total, of 148 new
388 regions larger than 1 kbp were identified in Ath-Nd-1_v2c. These regions are also more
389 frequent in proximity of the centromere (r=-0.43, $p=3.7*10^{-7}$).
390
391 **Hint-based gene prediction**
392 Hint-based gene prediction using AUGUSTUS with the *A. thaliana* species parameter set on
393 the Nd-1 pseudochromosomes resulted in 30,126 nuclear protein coding genes
394 (GeneSet_Nd-1_v2.0) with an average predicted transcript length of 1,798 bp, an average
395 predicted CDS length of 1,391 bp and an average exon number per predicted transcript of
396 5.98. The number of predicted genes is reduced compared to the GeneSet_Nd-1_v1.1 [39]
397 by 708 genes. In total, 28,042 (93%) representative peptide sequences were matched to
398 Araport11 sequences and functionally annotated based on Araport11 information
399 (AdditionalFile16). As controls we ran the gene prediction with same parameters on Col-0
400 and L*er* pseudochromosome sequences resulting in 30,352 genes and 29,302 genes,
401 respectively. There were only minor differences concerning the average transcript and CDS
402 length as well as the number of exons per gene.
403 Based on 35,636 TEs detected in Nd-1 (AdditionalFile8) 2,879 predicted Nd-1 genes were
404 flagged as putative TE genes (AdditionalFile17, AdditionalFile18). This number matches well
405 with the difference between the predicted genes in Nd-1 and the annotated protein coding
406 genes in Araport11, which is supposed to be free of TE genes. The predicted mRNAs were
407 supported by ESTs, which matched almost perfectly with an average similarity of 98.7%
408 (AdditionalFile19). Additionally, the assembly was screened for TEs resulting in 613
409 consensus sequences of TE families (https://doi.org/10.5447/IPK/2019/4).
410 The comparative gene prediction with CAT resulted in 26,717 genes in Nd-1 and 26,681
411 genes in L*er*, respectively. Average CDS lengths were 1,292 bp and 1,291 bp, respectively.
412 Since TE associated genes were not identified in this gene prediction process, the number of
413 gene models predicted by CAT should be smaller than the number predicted by

AUGUSTUS. The difference of 3,409 for Nd-1 is slightly exceeding the number of 2,879 TE associated genes that were predicted and flagged in the GeneSet_Nd-1_v2.0.

Besides protein encoding genes, 557 tRNA genes and 963 rRNA genes were predicted by INFERNAL. Comparison of these predicted tRNA genes to the result of tRNAscan-SE revealed an overlap of 552 (96.5%).

Detection of gene space differences between Nd-1 and Col-0

A BLASTp-based comparison of all predicted Nd-1 peptide sequences and Col-0 Araport11 representative peptide sequences in both directions revealed 24,453 reciprocal best hits (RBHs) (AdditionalFile20). In total, 89.1% of all 27,445 nuclear Col-0 genes are represented in this RBH set. Analysis of the colinearity of the genomic location of all 24,453 RBHs (see AdditionalFile21 for a list) between Nd-1 and Col-0 showed overall synteny of both genomes as well as an inversion on chromosome 4 (AdditionalFile22). While most RBHs are properly flanked by their syntenic homologs and thus lead to a diagonal positioning of points in the scatter plot, there are 345 outliers (see AdditionalFile23 for a list). In general, outliers occur frequently in regions around the centromeres. Positional analysis revealed an involvement of many outliers in the large inversion on chromosome 4. An NGS read mapping at the positions of randomly selected outliers was manually inspected and indicated rearrangements between Nd-1 and Col-0. Structural variants, which affect at least three different genes in a row of RBH pairs, were identified from the RBH analysis. Examples beside the previously mentioned 1.2 Mbp inversion on chromosome 4 (*At4g03820-At4g05497*) are a translocation on chromosome 3 (*At3g60975-At3g61035*) as well as an inversion on chromosome 3 around *At3g30845*.

As a control we identified 25,556 (91.1%) RBHs between our gene prediction on Col-0 and the manually curated reference annotation Araport11. In addition, 24,329 (88.6 %) RBHs were identified between our gene prediction on the L*er* assembly and the Col-0 annotation Araport11.

441 In total, 947 protein encoding genes in Nd-1 (AdditionalFile24) were detected to be copies of
442 only 421 genes annotated in Araport11. *SEC10* (*At5g12370*) [5] was previously described as
443 an example for a tandem gene duplication collapsed in the Col-0 gold standard sequence.
444 However, this region was already properly represented in AthNd-1_v1 [13]. Gene
445 duplications of *At2g06555* (unknown protein), *At3g05530* (*RPT5A*) and *At4g11510*
446 (*RALFL28*) in Nd-1 were confirmed by PCR amplification and Sanger sequencing of the
447 sequences enclosed by both copies as well as through amplification of the entire event locus.
448 On the other hand, there are 383 predicted genes in Nd-1 (AdditionalFile25) which appeared
449 at least duplicated in Col-0.
450
451 **Pan-genomic analyses**
452 Presence/absence variations of genes were inspected across a panel of 964 additional
453 accessions (https://doi.org/10.5447/IPK/2019/4). In total, 25,809 genes were present in
454 almost all accessions, 1,438 genes were considered dispensable, and the remaining 2,879
455 genes were flagged as TE or at least TE-associated genes (AdditionalFile26). Dispensable
456 genes and TE genes are frequently located in proximity of the centromeres while core genes
457 are less frequent in these regions (AdditionalFile27).
458
459 **Hidden locus in Col-0**
460 *At4g22214* was identified as a gene duplicated in Nd-1 in our analysis. During experimental
461 validation, we did not detect the expected difference between Col-0 and Nd-1 DNA
462 concerning the locus around *At4g22214*. However, the PCR results from Col-0 matched the
463 expectation based on the Nd-1 genome sequence thus suggesting a collapsed gene
464 sequence in the Col-0 gold standard sequence. This hypothesis was supported by PCR
465 results with outwards facing primers (Fig. 4). Cloning of the At4g22214 region of Col-0 in five
466 overlapping fragments was done to enable Sanger sequencing. The combination of Sanger
467 and paired-end Illumina sequencing reads revealed a tandem duplication with modification of
468 the original gene (Fig. 4). The copies were designated At4g22214a and At4g22214b based

469 on their position in the genome (GenBank: MG720229). While At4g22214b almost perfectly
470 matches the Araport11 annotation of At4g22214, a significant part of the CDS of At4g22214a
471 is missing. Therefore, the gene product of this copy is probably functionless. At4g22214 is
472 annotated as defensin-like family protein [55]. Since the family of defensin proteins contains
473 about 300 members in *A. thaliana* [55], the functional implications of this duplication are
474 probably low.
475
476 **Gaps in the Col-0 reference sequence**
477 Despite its very high quality, the Col-0 gold standard sequence contains 92 N stretches of
478 various sizes representing regions of unknown sequence like the NOR clusters or
479 centromeres. Ath-Nd1_v2c enabled the investigation of some of these sequences based on
480 homology assumptions. A total of 13 Col-0 gold standard sequence gaps were spanned with
481 high confidence by Ath-Nd1_v2c and therefore selected for homopolymer frequency
482 analysis. The corresponding regions in Nd-1 are significantly enriched with homopolymers in
483 comparison to randomly picked control sequences (p=0.000048, Mann-Whitney U test)
484 (AdditionalFile28).
485
486
487 **Discussion**
488 **Genome structure of the *A. thaliana* accession Nd-1**
489 In order to further investigate large variations in the range of several kbp up to several Mbp
490 between *A. thaliana* accessions, we performed a *de novo* genome assembly for the Nd-1
491 accession using long sequencing reads and cutting-edge assembly software. Based on
492 SMRT sequencing reads the assembly contiguity was improved by over 75 fold considering
493 the number of contigs in the previously released NGS-based assembly [13]. Assembly
494 statistics were comparable to other projects using similar data [11, 14, 15, 56, 57]. Despite
495 the very high contiguity, regions like NORs still pose a major challenge. These regions are
496 not just randomly clustered repeats, but highly controlled and ordered repetitions of

497 sequences [58]. Therefore, the identification of accession-specific sequence differences
498 could explain phenotypic differences. NOR repeat unit sequences in Ath-Nd-1_v2c are
499 located on the distal short arm of NdChr2 and NdChr4. This NOR position matches the
500 situation in Col-0 where the NOR2 is located distal on the short arm of Chr2 [59] and NOR4
501 on Chr4, respectively. In addition to NORs, the assembly of chromosome ends remains still
502 challenging, since the absence of some telomeric sequences in a high quality assembly was
503 observed before [14]. Despite the absence of challenging repeats, regions close to the
504 telomeres including the genes At3g01060 (BUSCO ID: EOG09360D4T) and At5g01010
505 (BUSCO ID: EOG09360DFK) were not assembled by FALCON (Ath-Nd1_v2f) although
506 sequence reads covering these regions were present in the input data. Also, this region is
507 represented in the Canu assembly (Ath-Nd1_v2c). In our hands, Canu performed best for the
508 assembly of the Nd-1 genome sequence based on SMRT sequencing reads.
509
510 **Nuclear genome sequence differences**
511 The increased contiguity of this long read assembly was necessary to discover an
512 approximately 1 Mbp inversion through sequence comparison as well as RBH analysis. An
513 earlier Illumina short read based assembly [13] lacked sufficient contiguity in the region of
514 interest to reveal both breakpoints of this variant between Col-0 and Nd-1. The large
515 inversion at the north of NdChr4 relative to the Col-0 gold standard sequence turned out as a
516 modification of the allele originally detected in L*er* [14, 60]. However, the Nd-1 allele is
517 different from the L*er* allele. This could explain previous observations in several hundred
518 *A. thaliana* accessions, which share the left inversion border with L*er*, but show a different
519 right inversion border [14].
520 Despite the very much improved contiguity and selection of Canu as the currently best
521 assembler for our dataset, there are only very small parts of pericentromeric sequences
522 represented in the Ath-Nd1_v2c assembly. Centromeric regions with an estimated size of 5
523 Mbp each [13] were not assembled. The absence of these highly repetitive regions is in
524 agreement with previous findings that the error rate of long reads is still too high to resolve

525 NORs and centromeres [15]. The pericentromeric and to a very limited extent also
526 centromeric regions are represented in the assemblies by small contigs of 50-100 kbp.
527 However, absence of telomeric sequences from some pseudochromsome ends was
528 observed before even for a very high quality assembly [14, 15]. The detected telomeric
529 repeats at the centromere positions support previously reported hypothesis about the
530 evolution of centromers out of telomere sequences [61], and telomeric or centromeric
531 sequences, respectively, at the end of at least some pseudochromosomes indicated the
532 completeness of the Ath-Nd1_v2c assembly at these points. However, almost 20 years after
533 the release of the first chromosome sequences of *A. thaliana*, we are still not able to
534 assemble complete centromere sequences continuously.
535 Sequence differences observed on the short arm of chromosome 2 between Col-0 and Nd-1
536 could be due to the integration of mtDNA into the Chr2 of Col-0 [2]. This region was reported
537 to be collapsed in the Col-0 reference genome sequence, harboring in real Col-0 DNA about
538 600 kbp of mtDNA instead of the 270 kbp represented in the reference genome sequence
539 [62]. However, Ath-Nd1_v2c did not reveal such a duplication of the mtDNA located in
540 NdChr2. Filtering of plastome and chondrome sequences during the polishing process could
541 be responsible for this if copies would have been fragmented into multiple contigs. In this
542 region, we detected in the Nd-1 assembly sequences unrelated to the corresponding Col-0
543 reference sequence. Since Nd-1 genes of this region show similarity to gene clusters on
544 other chromosomes, they could be relics of a whole genome duplication as reported before
545 for several regions of the Col-0 gold standard sequence [63]. This difference on Chr2 at
546 about 3.2 to 3.5 Mbp is only one example for a large variant region between Col-0 and Nd-1.
547 Similar though shorter such differences detected around centromeres could be explained by
548 TEs and pseudogenes which were previously reported as causes for intra-species variants in
549 these regions [62, 64].
550
551 **Plastome and chondrome**

552 Size and structure of the Nd-1 plastome is very similar to Col-0 [2] or L*er* [27]. In accordance
553 with the overall genome similarities, the observed number of small differences between the
554 plastome sequences of Col-0 and Nd-1 is slightly higher than the value reported before for
555 the Col-0 comparison to L*er* [27].
556 The size of the Nd-1 chondrome matches previously reported values for the large chondrome
557 configuration of other *A. thaliana* accessions [65]. Large structural differences between the
558 Col-0 chondrome [65] and the Nd-1 chondrome could be due to the previously described
559 high diversity of this subgenome including the generation of substoichiometric DNA
560 molecules [66, 67]. In addition, the mtDNA level was reported to differ between cell types or
561 cells of different ages within the same plant [68, 69]. The almost equal read coverage of the
562 assembled Nd-1 chondrome could be explained by the young age of the plants at the point of
563 DNA isolation, as the amount of all chondrome parts should be the same in young leafs [69].
564
565 **Nd-1 gene space**
566 Many diploid plant genomes contain on average around or even slightly below 30,000 protein
567 encoding genes [35, 70] with the *A. thaliana* genome harboring 27,445 nuclear protein-
568 coding genes according to the most recent Araport11 annotation [40]. Since there are only
569 few other chromosome-level assembly sequences of *A. thaliana* available at the moment, we
570 do not know the precise variation range of gene numbers between different accessions. The
571 number of 27,247 predicted non-TE genes in Nd-1 is further supported by the identification of
572 24,453 RBHs with the Araport11 [40] annotation of the Col-0 gold standard sequence. This
573 number exceeds the matches between Col-0 and Ler-0 [14]. Our chromosome-level
574 assembly further enhances the gene prediction quality since at least 89.1% of all Col-0
575 genes were recovered. This reinforces previous studies that also reported annotation
576 improvements through improved assembly quality [71]. The number of 35,636 TEs annotated
577 for Ath-Nd-1_v2c exceeds the number of 33,892 such elements identified in the previous
578 assembly version Ath-Nd-1_v1 [13] by 1,744. Such an increase in the number of resolved

579 TEs as well as an improved assembly of TE-rich regions in assemblies based on long reads
580 was reported before [72].
581 Due to the high proportion of genes within the *A. thaliana* genome assigned to paralogous
582 groups with high sequence similarity [73, 74], we speculated that the identification of
583 orthologous pairs via RBH analysis might be almost saturated. Gene prediction with the
584 same parameters on the Col-0 gold standard genome sequence prior to RBH analysis
585 supported this hypothesis. However, the incorporation of accession-specific RNA-Seq
586 derived hints could further increase the accuracy of the Nd-1 gene prediction. Since there are
587 even some RBHs at non-syntenic positions between the control Col-0 annotation and the
588 Araport11 annotation, our Nd-1 annotation is already of very high accuracy. The precise
589 annotation of non-canonical splice sites via hints as described before [39] contributed to the
590 new GeneSet_Nd-1_v2.0. Gene duplication and deletion numbers, or accession specific
591 presence/absence variations of genes, in Nd-1 and Col-0 are in the same range as
592 previously reported values of up to a few hundred [14, 75]. Since we were searching
593 genome-wide for copies of genes without requiring an annotated feature in each genome
594 sequence, both numbers might include some pseudogenes due to the frequent occurrence of
595 these elements within plant genomes [76, 77]. Since all comparisons rely on the constructed
596 sequences we cannot absolutely exclude that a small number of other genes were detected
597 as amplified due to collapsed sequences similar to SEC10 (At5g12370) [5]. Removing TE
598 genes based on sequence similarity to annotated features reduced the proportion of putative
599 pseudogenes. However, it is impossible to unequivocally distinguish between real genes and
600 pseudogenes in all cases, because even genes with a premature stop codon or a frameshift
601 mutation could function as a truncated version or give rise to regulatory RNAs [74, 77-79]. In
602 addition, the impact of copy number variations involving protein encoding genes in *A.*
603 *thaliana* might be higher than previously assumed thus supporting the existence of multiple
604 gene copies [80]. Gene expression analysis could support the discrimination of
605 pseudogenes, because low gene expression in *A. thaliana* was reported to be associated
606 with pseudogenization [81]. Despite the unclear status of the gene product, the mere

607 presence of these sequences revealed fascinating insights into genome evolution and
608 contributed to the pan-genome [82, 83].
609
610 **Conclusions**
611 We report a high quality long read *de novo* assembly (AthNd-1_v2c) of the *A. thaliana*
612 accession Nd-1, which improved significantly on the previously released NGS assembly
613 sequence AthNd-1_v1.0 [13]. Comparison of the GeneSet_Nd-1_v2.0 with the Araport11
614 nuclear protein coding genes revealed 24,453 RBHs supporting an overall synteny between
615 both *A. thaliana* accessions except for an approximately 1 Mbp inversion at the north of
616 chromosome 4. Moreover, large structural variants were identified in the pericentromeric
617 regions. Comparisons with the Col-0 gold standard sequence also revealed a collapsed
618 locus around At4g22214 in Col-0. Therefore, this work contributes to the increasing
619 *A. thaliana* pan-genome with significantly extended details about genomic rearrangements.
620
621 **List of abbreviations**
622 NGS next generation sequencing
623 NOR nucleolus organizing region
624 RBH reciprocal best hit
625 SMRT single molecule real time
626
627
628 **Declarations**
629 **Ethics approval and consent to participate**
630 Not applicable
631
632 **Consent for publication**
633 Not applicable
634

Availability of data and materials

The data sets supporting the results of this article are included within the article and its additional files. The Ath-Nd-1_v2 assemblies (Table 1) and derived files are available as external downloads from http://doi.org/10.5447/IPK/2019/4. Sequencing reads were submitted to the SRA (SRP066294). Python scripts developed and applied for this study are available on github: https://github.com/bpucker/Nd1_PacBio (http://doi.org/10.5281/zenodo.2590750).

Competing interest

The authors declare that they have no competing interest.

Funding

We acknowledge the financial support of the German Research Foundation (DFG) and the Open Access Publication Fund of Bielefeld University for the article processing charge. The funding body did not influence the design of the study, the data collection, the analysis, the interpretation of data, or the writing of the manuscript.

Author's contributions

BP, DH and BW conceived and designed research. BP, KS, KF, BH and RR conducted experiments. BP, DH and BW interpreted the data. BP and BW wrote the manuscript. All authors read and approved the final manuscript.

Acknowledgements

We thank Willy Keller for isolating high molecular DNA, Katharina Kemmet for extensive genotyping of plants for the genetic map, Helene Schellenberg, Ann-Christin Polikeit and Prisca Viehöver for Sanger sequencing, and Melanie Kuhlmann as well as Andrea Voigt for taking excellent care of the plants. We are very grateful for support from the Bioinformatics Resource Facility and Stefan Albaum.

663

664

665

666 **Additional Files**

667 **AdditionalFile1. Sequencing Statistics.**

668 Statistical information about the generated SMRT sequencing data for the *A. thaliana* Nd-1
669 genome assembly are listed in this table. The expected genome size is based on several
670 analyses reporting values around 150 Mbp [84, 85].

671

672 **AdditionalFile2. Canu assembly parameters.**

673 Listing of all parameters that were adjusted for the Canu assembly of the Nd-1 nucleome.
674 While most default parameters were kept, some were specifically adjusted for this plant
675 genome assembly.

676

677 **AdditionalFile3. FALCON assembly parameters.**

678 All parameters that were adjusted for the FALCON assembly of the Nd-1 nucleome are listed
679 in this table. While most default parameters were kept, some were specifically adjusted for
680 this plant genome assembly.

681

682 **AdditionalFile4. Molecular markers for genetic linkage analysis.**

683 All markers require the amplification of a genomic region using the listed oligonucleotides
684 under the specified conditions (annealing temperature, elongation time). Depending on the
685 fragment size differences, the resulting PCR products can allow the separation of both alleles
686 by agarose gel electrophoresis (length polymorphism) or might require Sanger sequencing to
687 investigate single SNPs.

688

689 **AdditionalFile5. Distribution of genetic markers over physical map.**

690 The positions of all genetic markers on the pseudochromosome sequences are illustrated.
691 Assembled sequences were positioned based on the genetic linkage information. Some
692 genetic marker combinations allowed the investigation of recombination frequencies within
693 continuous sequences.
694
695 **AdditionalFile6. Oligonucleotide sequences for genetic linkage analysis.**
696 Sequences, names and recommended annealing temperatures of all oligonucleotides used
697 in this work are listed in this table. Usage remarks for the oligonucleotides are provided as
698 well.
699
700 **AdditionalFile7. Alignment of Ath-Nd1_v2c and Ath-Nd1_v2f.**
701 Assemblies generated by Canu and FALCON, respectively, were compared via BLASTn
702 search of 10 kb sequence chunks. Color and position of dots in the figure indicate the
703 position of the best hit on the respective sequence.
704
705 **AdditionalFile8. TE positions in the Nd-1 genome sequence.**
706 TE genes, TEs, and TE fragments in the Nd-1 genome sequence were identified based on
707 sequence similarity to annotated TEs from the Col-0 gold standard sequence (Araport11)
708 [40].
709
710 **AdditionalFile9. BUSCO analysis of the Col-0 and Nd-1 genome sequences.**
711 BUSCO v2.0 was run on the genomic sequences of Col-0 and Nd-1 using AUGUSTUS 3.3
712 with default parameters for the gene prediction process.
713
714 **AdditionalFile10. Nd-1 plastome map.**
715 The GC content (black) and GC skew (green for positive GC skew, purple for negative GC
716 skew) of the plastome sequence were analyzed by CGView [31]. The sequence and its
717 properties are very similar to the Col-0 plastome sequence.

718

719 **AdditionalFile11. Nd-1 chondrome map.**

720 The GC content (black) and GC skew (green for positive GC skew, purple for negative GC
721 skew) of the chondrome sequence were analyzed by CGView [31]. The sequence and its
722 properties are very similar to the Col-0 chondrome sequence.

723

724 **AdditionalFile12. Experimental validation of 1 Mbp inversion on chromosome 4.**

725 The identified inversion between Nd-1 and Col-0 on chromosome 4 is different from the
726 inversion described before between Col-0 and L*er* [14]. However, the left breakpoint is the
727 same for both alleles enabling the use of previously published oligonucleotide sequences
728 [14]. The right breakpoint was identified by manual investigation of sequence alignments.
729 Both breakpoints were validated via PCR using the oligonucleotides (for sequences see
730 AdditionalFile6) as illustrated in (a). The results support the expected inversion borders (b).

731

732 **AdditionalFile13. Genome-wide distribution of genes inserted on chromosome 2 in Nd-**
733 **1.**

734 AthNd-1_v2c and the Col-0 gold standard sequence display a highly diverged region at the
735 north of chromosome 2, which is about 300 kbp long. BLASTn of the complete Nd-1 gene
736 sequences from this region revealed several regions on other Nd-1 chromosomes with
737 copies of these genes.

738

739 **AdditionalFile14. Genome-wide distribution of large structural variants.**

740 The distribution of structural variants (SVs) >10 kbp (red dots) between Col-0 and Nd-1 over
741 all five pseudochromosome sequences (black lines) is illustrated. Additionally, the assumed
742 centromere (CEN) positions are indicated (blue dots). Most SVs are clustered in the (peri-
743)centromeric region.

744

745 **AdditionalFile15. Clustering of SVs around centromeres.**

746 The correlation between the number of SVs in a given part of the genome sequence (1 Mbp)
747 and the distance of this region to the centromere position is illustrated. SVs are clustered
748 around the centromeres (Spearman correlation coefficient = -0.66, p-value = $1.7*10^{-16}$).

749

750 **AdditionalFile16. Functional annotation of GeneSet_Nd-1_v2.0.**

751 Functional annotations were transferred from Araport11 to corresponding RBHs in
752 GeneSet_Nd-1_v2.0. In addition, genes were annotated based on the best BLAST hit
753 if annotation via RBH was not possible.

754

755 **AdditionalFile17. TE overlap with GeneSet_Nd-1_v2.0.**

756 The overlap between annotated TEs (AdditionalFile8) and predicted protein coding genes
757 was analyzed to identify TE genes. This figure illustrates the fraction of a gene that is
758 covered by a TE. Since TEs might occur within the intron of a gene, only genes with at least
759 80% TE coverage were flagged as TE genes (AdditionalFile18).

760

761 **AdditionalFile18. TE genes in GeneSet_Nd-1_v2.0.**

762 These genes were predicted by AUGUSTUS as protein coding genes. Due to their positional
763 overlap with TEs (AdditionalFile8), they were flagged as TE genes and excluded from further
764 gene set analysis.

765

766 **AdditionalFile19. EST mapping.**

767 Percentage of nucleotides in ESTs matching predicted transcripts are displayed.

768

769 **AdditionalFile20. Gene set overlap between Araport11, GeneSet_Nd-1_v1.1, and**
770 **GeneSet_Nd-1_v2.0.**

771 RBHs were identified pairwise between gene sets. The overlap was identified by mapping all
772 genes onto Araport11 identifiers. Venn diagram construction was performed at
773 http://bioinformatics.psb.ugent.be/webtools/Venn/.

774

775 **AdditionalFile21. Reciprocal best hits (RBH) pairs between Col-0 and Nd-1.**

776 Reciprocal best hits between predicted peptide sequences of Nd-1 and the representative
777 peptide sequences of Col-0 (Araport11).

778

779 **AdditionalFile22. Reciprocal best hits (RHB) indicates inversion between Nd-1 and**
780 **Col-0.**

781 Genes in RBH pairs were sorted based on their position on the five pseudochromosomes of
782 the two genome sequences to form the x (Col-0) and y (Nd-1) axes of this diagram. Plotting
783 the positions of each RBH pair leads to a bisecting line of black dots representing genes at
784 perfectly syntenic positions. Red and green dots indicate RBH gene pair positions deviating
785 from the syntenic position. Red dots symbolize a unique match to another gene, while green
786 dots indicate multiple very similar matches. Positions of the centromere (CEN4) on the
787 chromosomes of both accessions are indicated by purple lines. An inversion involving 131
788 genes in RBH pairs just north of CEN4 distinguishes Nd-1 and Col-0.

789

790 **AdditionalFile23. RBH outliers in GeneSet_Nd-1_v2.0.**

791 RBHs between Araport11 and GeneSet_Nd-1_v2.0 were identified based on encoded
792 representative peptide sequences. All 242 RBHs at positions deviating from the syntenic
793 diagonal line were collected. The functional annotation of these genes was derived from
794 Araport11.

795

796 **AdditionalFile24. Duplicated genes in Nd-1.**

797 The listed 385 Col-0 genes (Araport11 [40]) have at least two copies in Nd-1. Exons of these
798 genes showed an increased copy number in Ath-Nd-1_v2c compared to the Col-0 gold
799 standard sequence. The annotation was derived from Araport11.

800

801 **AdditionalFile25. Duplicated genes in Col-0.**

802 The listed 394 Nd-1 genes have at least two copies in Col-0. Exons of these genes showed
803 an increased copy number in the Col-0 gold standard sequence compared to Ath-Nd-1_v2c.
804
805 **AdditionalFile26. Classification of genes as core, dispensable, or TE.**
806 GeneSet_Nd-1_v2.0 genes were classified as core, dispensable, or TE genes based on
807 coverage in a read mapping involving 1,137 Illumina read data sets.
808
809 **AdditionalFile27. Genome-wide distribution of core, dispensable, and TE genes.**
810 Visualisation of the position of core genes, dispensable genes and TEs along the
811 chromosomes.
812
813 **AdditionalFile28. Critical regions in the Col-0 gold standard sequence.**
814 The high contiguity of the Ath-Nd-1_v2c assembly enabled the investigation of 13 sequences
815 corresponding to gaps in the Col-0 gold standard sequence. This figure illustrates the
816 homotetranucleotide occurrence in these sequences (red dots) in comparison to some
817 randomly selected reference sequences (green dots). While there is a clear enrichment of
818 homotetranucleotides in the gap-homolog sequences, there was no clear correlation
819 between the length of a gap and the composition of the corresponding sequence observed.
820

References

1. Koornneef M, Meinke D. The development of Arabidopsis as a model plant. The Plant Journal. 2010;61(6):909-21.
2. The Arabidopsis Genome Initiative. Analysis of the genome sequence of the flowering plant *Arabidopsis thaliana*. Nature. 2000;408(6814):796-815.
3. Kumekawa N, Hosouchi T, Tsuruoka H, Kotani H. The size and sequence organization of the centromeric region of arabidopsis thaliana chromosome 5. DNA Research. 2000;7(6):315-21.
4. Long Q, Rabanal FA, Meng D, Huber CD, Farlow A, Platzer A, et al. Massive genomic variation and strong selection in Arabidopsis thaliana lines from Sweden. Nature Genetics. 2013;45(8):884-90. Epub 2013 Jun 23.
5. Vukašinović N, Cvrčková F, Eliáš M, Cole R, Fowler JE, Žárský V, et al. Dissecting a hidden gene duplication: the Arabidopsis thaliana SEC10 locus. PLoS ONE. 2014;9(4):e94077.
6. Kawakatsu T, Huang SS, Jupe F, Sasaki E, Schmitz RJ, Urich MA, et al. Epigenomic Diversity in a Global Collection of Arabidopsis thaliana Accessions. Cell. 2016;166(2):492-505.
7. Schneeberger K, Ossowski S, Ott F, Klein JD, Wang X, Lanz C, et al. Reference-guided assembly of four diverse Arabidopsis thaliana genomes. Proceedings of the National Academie of Sciences of the United States of America. 2011;108(25):10249-54. Epub 2011 Jun 6.
8. Li YH, Zhou G, Ma J, Jiang W, Jin LG, Zhang Z, et al. De novo assembly of soybean wild relatives for pan-genome analysis of diversity and agronomic traits. Nature Biotechnology. 2014;32(10):1045-54. Epub 2014 Sep 14.
9. Consortium TG. 1,135 Genomes Reveal the Global Pattern of Polymorphism in Arabidopsis thaliana. Cell. 2016;166(2):481-91. Epub 2016 Jun 9.
10. Kim KE, Peluso P, Babayan P, Yeadon PJ, Yu C, Fisher WW, et al. Long-read, whole-genome shotgun sequence data for five model organisms. Scientific Data. 2014;1:140045.
11. Berlin K, Koren S, Chin CS, Drake JP, Landolin JM, Phillippy AM. Assembling large genomes with single-molecule sequencing and locality-sensitive hashing. Nature Biotechnology. 2015;33(6):623-30. Epub 2015 May 25.
12. Chin CS, Peluso P, Sedlazeck FJ, Nattestad M, Concepcion GT, Clum A, et al. Phased diploid genome assembly with single-molecule real-time sequencing. Nature Methods. 2016;13(12):1050-4. Epub 2016 Oct 17.
13. Pucker B, Holtgräwe D, Rosleff Sörensen T, Stracke R, Viehöver P, Weisshaar B. A De Novo Genome Sequence Assembly of the Arabidopsis thaliana Accession Niederzenz-1 Displays Presence/Absence Variation and Strong Synteny. PLoS ONE. 2016;11(10):e0164321.
14. Zapata L, Ding J, Willing EM, Hartwig B, Bezdan D, Jiao WB, et al. Chromosome-level assembly of Arabidopsis thaliana Ler reveals the extent of translocation and inversion polymorphisms. Proceedings of the National Academy of Sciences of the United States of America. 2016.
15. Michael TP, Jupe F, Bemm F, Motley ST, Sandoval JP, Lanz C, et al. High contiguity Arabidopsis thaliana genome assembly with a single nanopore flow cell. Nature Communications. 2018;9(1):541.
16. Huddleston J, Chaisson MJP, Steinberg KM, Warren W, Hoekzema K, Gordon D, et al. Discovery and genotyping of structural variation from long-read haploid genome sequence data. Genome Research. 2017;27(5):677-85. Epub 2016 Nov 28.
17. Simpson JT, Pop M. The Theory and Practice of Genome Sequence Assembly. Annual Review of Genomics and Human Genetics. 2015;16:153-72. Epub 2015 Apr 22.
18. Rhoads A, Au KF. PacBio Sequencing and Its Applications. Genomics Proteomics Bioinformatics. 2015;13(5):278-89. Epub 2015 Nov 2.

19. Lam KK, Khalak A, D. T. Near-optimal assembly for shotgun sequencing with noisy reads. BMC Bioinformatics. 2014;15:S4. Epub 2014 Sep 10. doi: 10.1186/1471-2105-15-S9-S4.
20. Koren S, Phillippy AM. One chromosome, one contig: complete microbial genomes from long-read sequencing and assembly. Current Opinion in Microbiology. 2015;23:110-20. Epub 2014 Dec 1.
21. Shoromony I, Courtade T, Tse D. Do Read Errors Matter for Genome Assembly? IEEE International Symposium on Information Theory (ISIT); Hong Kong2015. p. 919-23.
22. Koren S, Harhay GP, Smith TP, Bono JL, Harhay DM, Mcvey SD, et al. Reducing assembly complexity of microbial genomes with single-molecule sequencing. Genome Biology. 2013;14(9):R101.
23. Pendleton M, Sebra R, Pang AW, Ummat A, Franzen O, Rausch T, et al. Assembly and diploid architecture of an individual human genome via single-molecule technologies. Nature Methods. 2015;12(8):780-6. Epub 2015 Jun 29.
24. Payne A, Holmes N, Rakyan V, Loose M. BulkVis: a graphical viewer for Oxford nanopore bulk FAST5 files. Bioinformatics. 2018.
25. Istace B, Friedrich A, d'Agata L, Faye S, Payen E, Beluche O, et al. de novo assembly and population genomic survey of natural yeast isolates with the Oxford Nanopore MinION sequencer. Gigascience. 2017;6(2):1-13.
26. Healey A, Furtado A, Cooper T, Henry RJ. Protocol: a simple method for extracting next-generation sequencing quality genomic DNA from recalcitrant plant species. Plant Methods. 2014;10(21). doi: 10.1186/1746-4811-10-21.
27. Stadermann KB, Holtgräwe D, Weisshaar B. Chloroplast Genome Sequence of Arabidopsis thaliana Accession Landsberg erecta, Assembled from Single-Molecule, Real-Time Sequencing Data. Genome Announcements. 2016;4(5):e00975-16.
28. Koren S, Walenz BP, Berlin K, Miller JR, Bergman NH, Phillippy AM. Canu: scalable and accurate long-read assembly via adaptive k-mer weighting and repeat separation. Genome Research. 2017;27(5):722-36. Epub 2017 Mar 15.
29. Boetzer M, Henkel CV, Jansen HJ, Butler D, Pirovano W. Scaffolding pre-assembled contigs using SSPACE. Bioinformatics. 2011;27(4):578-9. Epub 2010 Dec 12.
30. Kleinboelting N, Huep G, Appelhagen I, Viehoever P, Li Y, Weisshaar B. The Structural Features of Thousands of T-DNA Insertion Sites Are Consistent with a Double-Strand Break Repair-Based Insertion Mechanism. Molecular Plant. 2015;8(11):1651-64. Epub 2015 Sep 5.
31. Stothard P, Wishart DS. Circular genome visualization and exploration using CGView. Bioinformatics. 2005;21(4):537-9. Epub 2004 Oct 12.
32. Kolmogorov M, Yuan J, Lin YR, Pevzner PA. Assembly of Loing Error-Prone Reads Using Repeat Graphs. 2018.
33. Li H. Minimap and miniasm: fast mapping and de novo assembly for noisy long sequences. Bioinformatics. 2016;32(14):2103-10. Epub 2016 Mar 19.
34. Li H. Aligning sequence reads, clone sequences and assembly contigs with BWA-MEM. Oxford University Press. 2013:1-3.
35. Pucker B, Brockington SF. Genome-wide analyses supported by RNA-Seq reveal non-canonical splice sites in plant genomes. BMC Genomics. 2018;19(1):980.
36. Walker BJ, Abeel T, Shea T, Priest M, Abouelliel A, Sakthikumar S, et al. Pilon: an integrated tool for comprehensive microbial variant detection and genome assembly improvement. PLoS ONE. 2014;9(11):e112963.
37. Untergasser A, Nijveen H, Rao X, Bisseling T, Geurts R, Leunissen JA. Primer3Plus, an enhanced web interface to Primer3. Nucleic acids research. 2007;35:W71-4. Epub 2007 May 7.
38. Rosso MG, Li Y, Strizhov N, Reiss B, Dekker K, Weisshaar B. An *Arabidopsis thaliana* T-DNA mutagenised population (GABI-Kat) for flanking sequence tag based reverse genetics. Plant Molecular Biology. 2003;53(1):247-59.
39. Pucker B, Holtgräwe D, Weisshaar B. Consideration of non-canonical splice sites improves gene prediction on the Arabidopsis thaliana Niederzenz-1 genome sequence. BMC Research Notes. 2017;10(1):667.

931 40. Cheng CY, Krishnakumar V, Chan A, Thibaud-Nissen F, Schobel S, Town CD.
932 Araport11: a complete reannotation of the Arabidopsis thaliana reference genome. The Plant
933 Journal. 2017;(89):789-804.
934 41. Arend D, Junker A, Scholz U, Schüler D, Wylie J, Lange M. PGP repository: a plant
935 phenomics and genomics data publication infrastructure. Database. 2016.
936 42. Simão FA, Waterhouse RM, Ioannidis P, Kriventseva EV, Zdobnov EM. BUSCO:
937 assessing genome assembly and annotation completeness with single-copy orthologs.
938 Bioinformatics. 2015;31(19):3210-2. Epub 2015 Jun 9.
939 43. Kurtz S, Phillippy A, Delcher AL, Smoot M, Shumway M, Antonescu C, et al. Versatile
940 and open software for comparing large genomes. Genome Biology. 2004;5(2):R12. Epub
941 2004 Jan 30.
942 44. Khelik K, Lagesen K, Sandve GK, Rognes T, Nederbragt AJ. NucDiff: in-depth
943 characterization and annotation of differences between two sets of DNA sequences. BMC
944 Bioinformatics. 2017;18(1):338.
945 45. Keller O, Kollmar M, Stanke M, Waack S. A novel hybrid gene prediction method
946 employing protein multiple sequence alignments. Bioinformatics. 2011;27(6):757-63. Epub
947 2011 Jan 6.
948 46. Schmid KJ, Sorensen TR, Stracke R, Torjek O, Altmann T, Mitchell-Olds T, et al.
949 Large-scale identification and analysis of genome-wide single-nucleotide polymorphisms for
950 mapping in *Arabidopsis thaliana*. Genome Research. 2003;13(6A):1250-7. Epub 2003/06/12.
951 doi: 10.1101/gr.728603. PubMed PMID: 12799357.
952 47. Altschul SF, Gish W, Miller W, Myers EW, Lipman DJ. Basic local alignment search
953 tool. Journal of molecular biology. 1990;215(3):403-10.
954 48. Katoh K, Standley DM. MAFFT multiple sequence alignment software version 7:
955 improvements in performance and usability. Molecular Biology and Evolution.
956 2013;30(4):772-80. Epub 2013 Jan 16.
957 49. Smit AFA, Hubley R, Green P. RepeatMasker Open-4.0 2013-2015. Available from:
958 http://www.repeatmasker.org.
959 50. Paten B, Earl D, Nguyen N, Diekhans M, Zerbino D, Haussler D. Cactus: Algorithms
960 for genome multiple sequence alignment. Genome Research. 2011;21(9):1512-28. Epub
961 2011 Jun 10.
962 51. Fiddes IT, Armstrong J, Diekhans M, Nachtweide S, Kronenberg ZN, Underwood JG,
963 et al. Comparative Annotation Toolkit (CAT)-simultaneous clade and personal genome
964 annotation. Genome Research. 2018;28(7):1029-38. Epub 2018 Jun 8.
965 52. Nawrocki EP, Eddy SR. Infernal 1.1: 100-fold faster RNA homology searches.
966 Bioinformatics. 2013;29(22):2933-5. Epub 2013 Sep 4.
967 53. Kalvari I, Argasinska J, Quinones-Olvera N, Nawrocki EP, Rivas E, Eddy SR, et al.
968 Rfam 13.0: shifting to a genome-centric resource for non-coding RNA families. Nucleic acids
969 research. 2018;46(D1):D335-D42.
970 54. Lowe TM, Eddy SR. tRNAscan-SE: a program for improved detection of transfer RNA
971 genes in genomic sequence. Nucleic acids research. 1997;25(5):955-64.
972 55. Silverstein KA, Graham MA, Paape TD, VandenBosch KA. Genome organization of
973 more than 300 defensin-like genes in Arabidopsis. Plant Physiology. 2005;138(2):600-10.
974 56. Cho YS, Kim H, Kim HM, Jho S, Jun J, Lee YJ, et al. An ethnically relevant
975 consensus Korean reference genome is a step towards personal reference genomes. Nature
976 Communications7. 2016:13637.
977 57. Seo JS, Rhie A, Kim J, Lee S, Sohn MH, Kim CU, et al. De novo assembly and
978 phasing of a Korean human genome. Nature. 2016;538(7624):243-7. Epub 2016 Oct 5.
979 58. Chandrasekhara C, Mohannath G, Blevins T, Pontvianne F, Pikaard CS.
980 Chromosome-specific NOR inactivation explains selective rRNA gene silencing and dosage
981 control in Arabidopsis. Genes & Development. 2016;30(2):177-90. Epub 2016 Jan 7.
982 59. Copenhaver GP, Pikaard CS. RFLP and physical mapping with an rDNA-specific
983 endonuclease reveals that nucleolus organizer regions of Arabidopsis thaliana adjoin the
984 telomeres on chromosomes 2 and 4. The Plant Journal. 1996;9(2):259-72.

985 60. Hu TT, Pattyn P, Bakker EG, Cao J, Cheng JF, Clark RM, et al. The Arabidopsis
986 lyrata genome sequence and the basis of rapid genome size change. Nature Genetics.
987 2011;43(5):476-81. Epub 2011 Apr 10.
988 61. Villasante A, Abad JP, Méndez-Lago M. Centromeres were derived from telomeres
989 during the evolution of the eukaryotic chromosome. Proceedings of the National Academy of
990 Sciences of the United Stated of America. 2007;104(25):10542-7. Epub 2007 Jun 8.
991 62. Stupar RM, Lilly JW, Town CD, Cheng Z, Kaul S, Buell CR, et al. Complex mtDNA
992 constitutes an approximate 620-kb insertion on Arabidopsis thaliana chromosome 2:
993 implication of potential sequencing errors caused by large-unit repeats. Proceedings of the
994 National Academy of Sciences of the United Stated of America. 2001;98(9):5099-103. Epub
995 2001 Apr 17.
996 63. Kowalski SP, Lan TH, Feldmann KA, Paterson AH. Comparative mapping of
997 Arabidopsis thaliana and Brassica oleracea chromosomes reveals islands of conserved
998 organization. Genetics. 1994;138(2):499-510.
999 64. Fransz PF, Armstrong S, de Jong JH, Parnell LD, van Drunen C, Dean C, et al.
1000 Integrated cytogenetic map of chromosome arm 4S of A. thaliana: structural organization of
1001 heterochromatic knob and centromere region. Cell. 2000;100(3):367-76.
1002 65. Unseld M, Marienfeld JR, Brandt P, Brennicke A. The mitochondrial genome of
1003 Arabidopsis thaliana contains 57 genes in 366,924 nucleotides. Nature Genetics.
1004 1997;15(1):57-61.
1005 66. Martínez-Zapater JM, Gil P, Capel J, Somerville CR. Mutations at the Arabidopsis
1006 CHM locus promote rearrangements of the mitochondrial genome. The Plant Cell.
1007 1992;4(8):889-99.
1008 67. Christensen AC. Plant mitochondrial genome evolution can be explained by DNA
1009 repair mechanisms. Genome Biology and Evolution. 2013;5(6):1079-86.
1010 68. Preuten T, Cincu E, Fuchs J, Zoschke R, Liere K, Börner T. Fewer genes than
1011 organelles: extremely low and variable gene copy numbers in mitochondria of somatic plant
1012 cells. The Plant Journal. 2010;64(6):948-59. Epub 2010 Nov 4.
1013 69. Woloszynska M, Gola EM, Piechota J. Changes in accumulation of heteroplasmic
1014 mitochondrial DNA and frequency of recombination via short repeats during plant lifetime in
1015 Phaseolus vulgaris. Acta Biochimica Polonica. 2012;59(4):703-9. Epub 2012 Dec 6.
1016 70. Wendel JF, Jackson SA, Meyers BC, Wing RA. Evolution of plant genome
1017 architecture. Genome Biology. 2016;17(37):s13059-016-0908-1.
1018 71. Denton JF, Lugo-Martinez J, Tucker AE, Schrider DR, Warren WC, Hahn MW.
1019 Extensive error in the number of genes inferred from draft genome assemblies. PLoS
1020 Computational Biology. 2014;10(12):e1003998.
1021 72. Belser C, Istace B, Denis E, Dubarry M, Baurens FC, Falentin C, et al. Chromosome-
1022 scale assemblies of plant genomes using nanopore long reads and optical maps. Natural
1023 Plants. 2018;4(11):879-87. Epub 2018 Nov 2.
1024 73. Paquette SM, Bak S, Feyereisen R. Intron-exon organization and phylogeny in a
1025 large superfamily, the paralogous cytochrome P450 genes of Arabidopsis thaliana. DNA and
1026 Cell Biology. 2000;19(5):307-17.
1027 74. Panchy N, Lehti-Shiu M, Shiu SH. Evolution of Gene Duplication in Plants. Plant
1028 Physiology. 2016;171(4):2294-316. Epub 2016 Jun 10.
1029 75. Tan S, Zhong Y, Hou H, Yang S, Tian D. Variation of presence/absence genes
1030 among Arabidopsis populations. BMC Evolutionary Biology. 2012;12(86):1471-2148/12/86.
1031 76. Benovoy D, Drouin G. Processed pseudogenes, processed genes, and spontaneous
1032 mutations in the Arabidopsis genome. Journal of Molecular Evolution. 2006;62(5):511-22.
1033 Epub 2006 Apr 11.
1034 77. Zou C, Lehti-Shiu MD, Thibaud-Nissen F, Prakash T, Buell CR, Shiu SH. Evolutionary
1035 and expression signatures of pseudogenes in Arabidopsis and rice. Plant Physiology.
1036 2009;151(1):3-15. Epub 2009 Jul 29.
1037 78. Yamada K, Lim J, Dale JM, Chen H, Shinn P, Palm CJ, et al. Empirical analysis of
1038 transcriptional activity in the Arabidopsis genome. Science. 2003;302(5646):842-6.
1039 79. Siena LA, Ortiz JP, Calderini O, Paolocci F, Cáceres ME, Kaushal P, et al. An
1040 apomixis-linked ORC3-like pseudogene is associated with silencing of its functional homolog

in apomictic Paspalum simplex. Journal of Experimental Botany. 2016;67(6):1965-78. Epub 2016 Feb 2.

80. Zmienko A, Samelak-Czajka A, Kozlowski P, Szymanska M, Figlerowicz M. Arabidopsis thaliana population analysis reveals high plasticity of the genomic region spanning MSH2, AT3G18530 and AT3G18535 genes and provides evidence for NAHR-driven recurrent CNV events occurring in this location. BMC Genetics. 2016;17(1):893.

81. Yang L, Takuno S, Waters ER, Gaut BS. Lowly expressed genes in Arabidopsis thaliana bear the signature of possible pseudogenization by promoter degradation. Molecular Biology and Evolution. 2011;28(3):1193-203. Epub 2010 Nov 8.

82. Marroni F, Pinosio S, Morgante M. Structural variation and genome complexity: is dispensable really dispensable? Current Opinion in Plant Biology. 2014;18:31-6. Epub 2014 Feb 16.

83. Golicz AA, Batley J, Edwards D. Towards plant pangenomics. Plant Biotechnology Journal. 2016;14(4):1099-105. Epub 2015 Nov 23.

84. Arumuganathan K, Earle ED. Nuclear DNA Content of Some Important Plant Species. Plant Molecular Biology Reporter. 1991;9(3):208-18.

85. Höfte H, Desprez T, Amselm L, Chiapello H, Caboche M, Moisan A, et al. An inventory of 1152 expressed sequence tags obtained by partial sequencing of cDNAs from *Arabidopsis thaliana*. The Plant Journal. 1993;4(6):1051-61.

Figure Legends

Figure 1: Nd-1 genome structure.

Schematic pseudochromosomes are represented by black lines with positions of genomics features highlighted with colored icons as indicated in the insert.

Figure 2: Inversion on chromosome 4.

The dotplot heatmaps show the similarity between small fragments of two sequences. Each dot indicates a match of 1 kbp between both sequences, while the color is indicating the similarity of the matching sequences. A red line highlights an inversion between Nd-1 and Col-0 or L*er* and Col-0, respectively. A red arrow points at the position where the inversion alleles differ between Nd-1 and L*er*. (a) Comparison of the Nd-1 genome sequence against the Col-0 gold standard sequence reveals a 1 Mbp inversion. (b) The L*er* genome sequence displays another inversion allele [14].

Figure 3: Highly divergent region on chromosome 2.

There is a very low similarity region (light blue) between the sequences in region A and almost no similarity between the sequences in region B (white). The complete region between 3.29 Mbp and 3.48 Mbp on NdChr2 is missing in the L*er* genome.

Figure 4: Hidden locus in the Col-0 reference sequence.

Differences between the Nd-1 and Col-0 genome sequences lead to the discovery of a collapsed region in the Col-0 gold standard sequence. There are two copies of At4g22214 (blue) present in the Col-0 genome, while only one copy is represented in the Col-0 gold standard sequence. This gene duplication was initially validated through PCR with outwards

facing oligonucleotides N258 and N259 (purple) which lead to the formation of the expected PCR product (black). Parts of this region were cloned into plasmids (grey) for sequencing. Sanger and paired-end Illumina sequencing reads revealed one complete gene (At4g22214b) and a degenerated copy (At4g22214a). Moreover, the region downstream of the complete gene copy in Nd-1 indicates the presence of at least one additional degenerated copy.

Table 1: Nd-1 *de novo* assembly statistics.

Metrics of assemblies of the Nd-1 nucleome sequence generated by Canu, FALCON, miniasm, and Flye. All described assemblies are the final version after polishing.

parameter	**Ath-Nd1_v2c**	**Ath-Nd-1_v2f**	**Ath-Nd-1_v2m**	**Ath-Nd-1_v2y**
Assembler	Canu	FALCON	Miniasm	Flye
number of contigs	69	26	72	44
total number of bases	123,513,866	119,540,544	120,159,079	116,964,092
average contig length	1,790,056 bp	4,597,713 bp	1,668,876 bp	2,658,274 bp
minimal contig length	50,345 bp	86,055 bp	50,142 bp	53,207 bp
maximal contig length	15,898,009 bp	15,877,978 bp	14,338,505 bp	14,857,908 bp
GC content	36.14 %	36.04%	36.07%	36.01%
N25	14,369,729 bp	14,534,675 bp	11,880,610 bp	12,510,540 bp
N50	13,422,481 bp	9,302,209 bp	8,595,164 bp	10,607,548 bp
N75	8,555,326 bp	6,666,836 bp	3,513,050 bp	6,001,858 bp
N90	2,928,047 bp	2,829,734 bp	1,430,525 bp	2,524876 bp

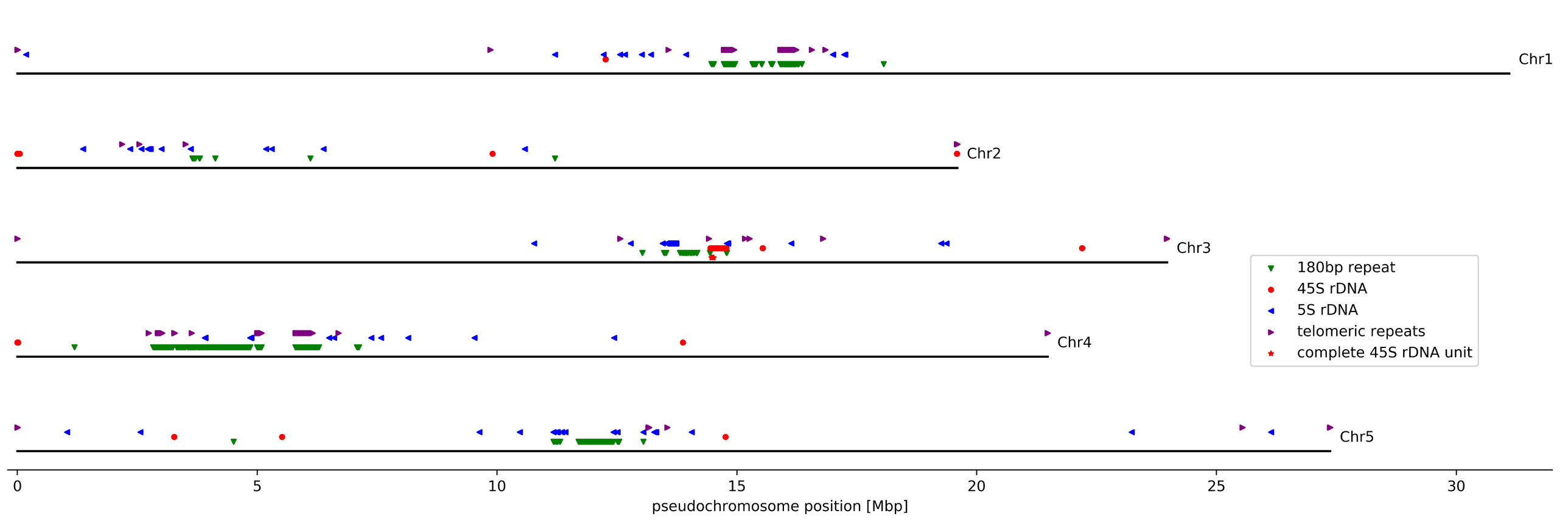
Chr1
Chr2
Chr3
Chr4
Chr5
180bp repeat
45S rDNA
5S rDNA
telomeric repeats
complete 45S rDNA unit
0
5
10
15
20
25
30
pseudochromosome position [Mbp]

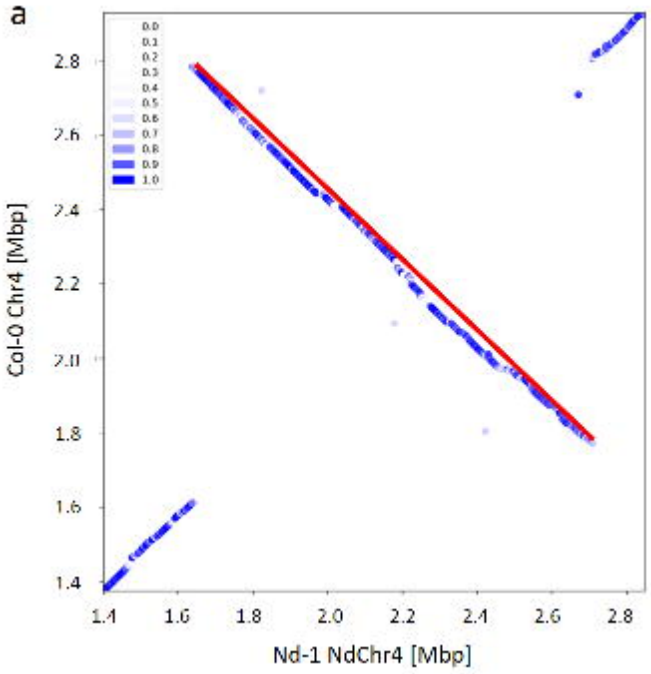
a
Col-0 Chr4 [Mbp]
Nd-1 NdChr4 [Mbp]
1.4
1.6
1.8
2.0
2.2
2.4
2.6
2.8

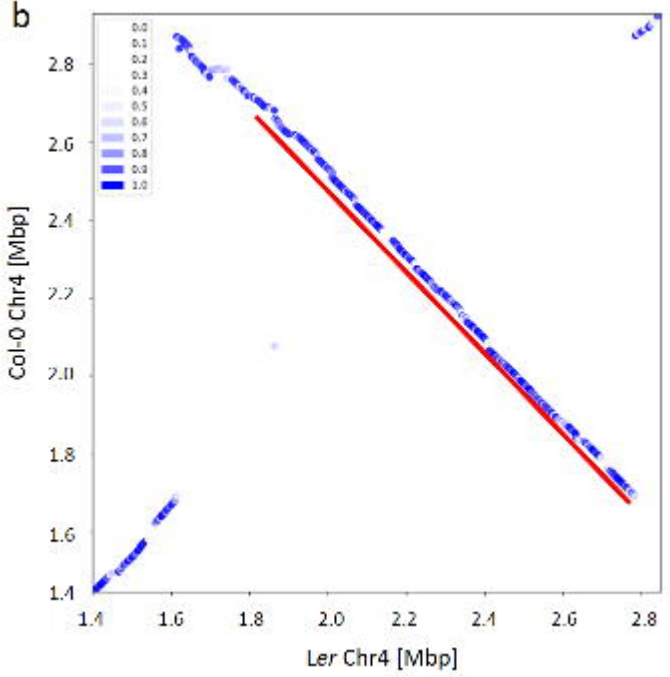
b
Col-0 Chr4 [Mbp]
Ler Chr4 [Mbp]
1.4
1.6
1.8
2.0
2.2
2.4
2.6
2.8

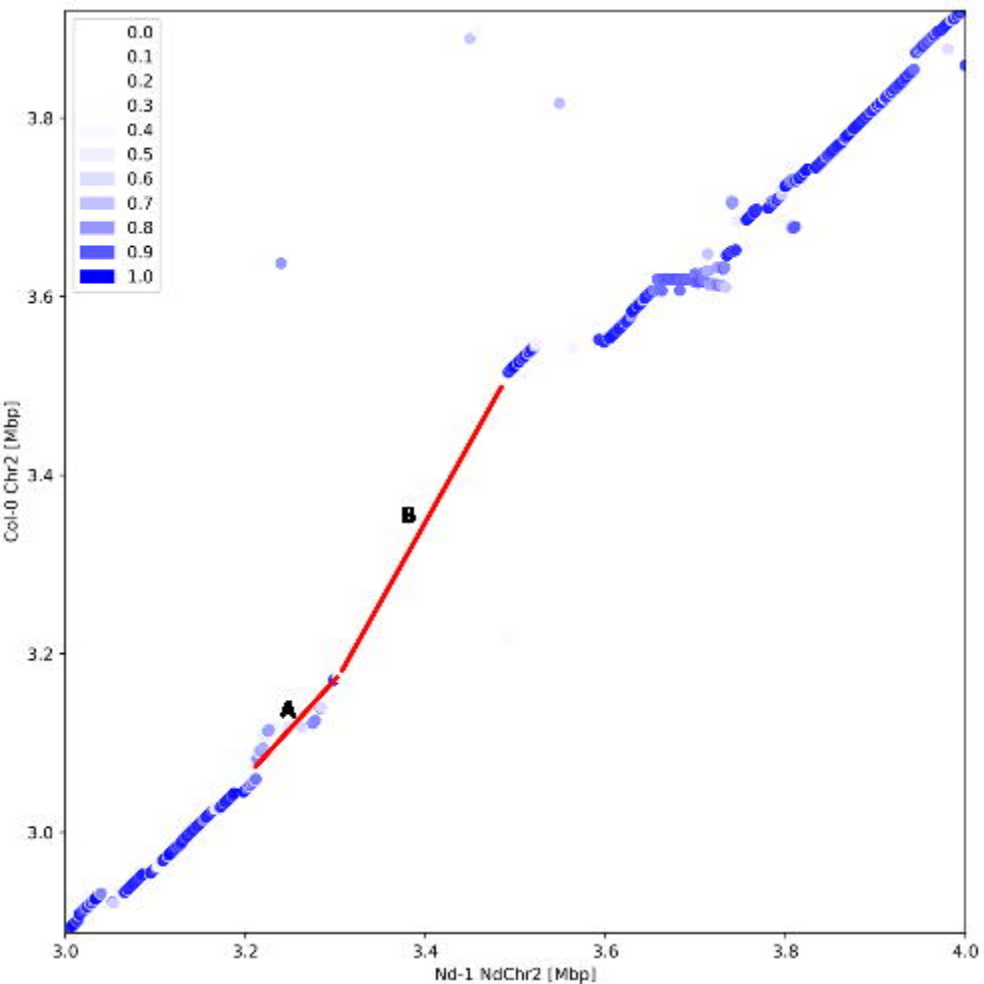
0.0
0.1
0.2
0.3
0.4
0.5
0.6
0.7
0.8
0.9
1.0
A
B
3.0
3.2
3.4
3.6
3.8
4.0
Col-0 Chr2 [Mbp]
Nd-1 NdChr2 [Mbp]

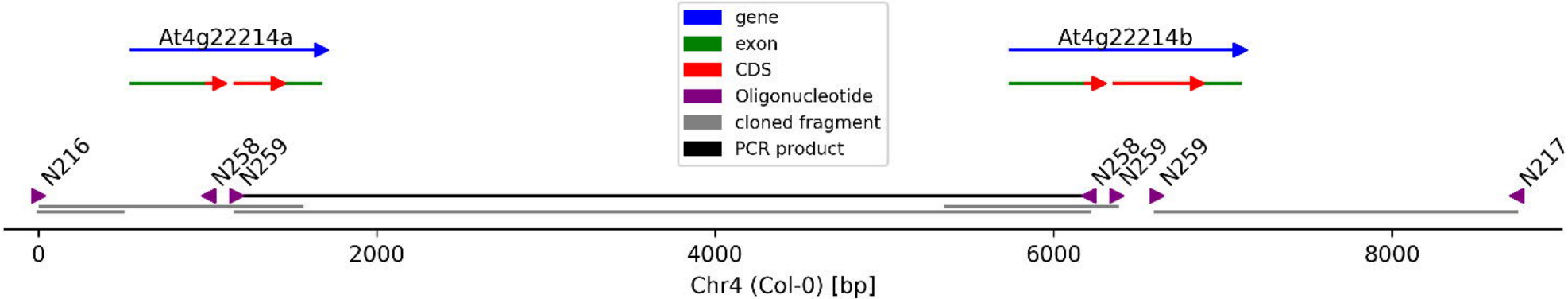
gene
exon
CDS
Oligonucleotide
cloned fragment
PCR product
At4g22214a
At4g22214b
N216
N258
N259
N258
N259
N259
N217
0
2000
4000
6000
8000
Chr4 (Col-0) [bp]